analytical chemistry

pubs.acs.org/ac Article

Universal and Programmable Rolling Circle Amplification-CRISPR/Cas12a-Mediated Immobilization-Free Electrochemical Biosensor

Min Qing, Sheng Liang Chen, Zhe Sun, Yi Fan, Hong Qun Luo,* and Nian Bing Li*

Cite This: *Anal. Chem.* 2021, 93, 7499−7507 Read Online

ACCESS | Metrics & More | Article Recommendations | Supporting Information

ABSTRACT: The development of a sensing platform with high sensitivity and specificity, especially programmability and universal applicability, for the detection of clinically relevant molecules is highly valuable for disease monitoring and confirmation but remains a challenge. Here, for the first time, we introduce the clustered regularly interspaced short palindromic repeats (CRISPR)/Cas system into an immobilization-free electrochemical biosensing platform for sensitively and specifically detecting the disease-related nucleic acids and small molecules. In this strategy, a modular rolling circle amplification (RCA) is designed to transform and amplify the target recognition event into the universal trigger DNA strand that is used as the trigger to activate the deoxyribonuclease activity of CRISPR/Cas12a for further signal amplification. The cleavage of the target-activated blocker probe allows the methylene blue-labeled reporter probes to be captured by the reduced graphene oxide-modified electrode, leading to an obviously increased electrochemical signal. We only need to simply tune the sequence for target recognition in RCA components, and this strategy can be flexibly applied to the highly sensitive and specific detection of microRNAs, Parvovirus B19 DNA, and adenosine-5′-triphosphate and the calculated limit of detection is 0.83 aM, 0.52 aM, and 0.46 pM, respectively. In addition, we construct DNA logic circuits (YES, NOT, OR, AND) of DNA inputs to experimentally demonstrate the modularity and programmability of the stimuli-responsive RCA-CRISPR/Cas12a system. This work broadens the application of the CRISPR/Cas12a system to the immobilization-free electrochemical biosensing platform and provides a new thinking for developing a robust tool for clinical diagnosis.

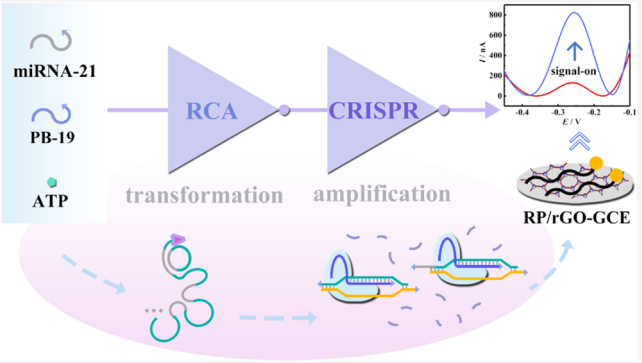

INTRODUCTION

The ability to rapidly detect clinically relevant molecules, including proteins, nucleic acids, and small molecules, with high specificity and sensitivity at point-of-care (POC) settings is crucial for disease monitoring and confirmation, epidemiology, and general laboratory tasks.[1,2] Much efforts have been devoted to developing ingenious diagnostic technologies; unfortunately, they have trade-offs in cost-effectiveness, portability, ease of use, flexibility, analytic sensitivity, and specificity. Recently, the clustered regularly interspaced short palindromic repeats (CRISPR)/Cas system, that is, guide RNA directs the Cas protein to specific target nucleic acid for activating its nuclease activity, not only have launched a blast of upsurge in genome editing but also have given rise to the innovation of molecular diagnostics technology.[3,4] The CRISPR/Cas system coupled with the polymerase chain reaction and various isothermal amplifications, based on the transduction of target-activated collateral cleavage of reporter probes into a fluorescence signal output, have been exploited as robust diagnostic tools.[5−14] Considering that these optical transduction-based assays require to be operated in expensive and sophisticated equipment, it is necessary to extend the CRISPR/Cas system to electrochemical biosensing.

Electrochemical techniques combined with the specific CRISPR/Cas system have the potential to mitigate the key challenge of POC diagnostics due to its attractive features, including high sensitivity, rapid signal readout, simple and cost-effective transduction elements, easy integration with additional components, and the potential for miniaturization.[15−17] Despite their great success, they suffer from some limitations as follows. In contrast to optical approaches operated in a homogeneous solution, the reported electrochemical biosensing platforms require probe surface immobilization and, more importantly, elaborate the optimization of surface chemistry and coverage; however, such laborious optimization and time-consuming manipulation are not competitive to fulfill the repeatability of analysis and the requirements of POC.[18−20] Also, the environment-sensitive configurational freedom of the

Received: February 22, 2021
Accepted: May 3, 2021
Published: May 13, 2021

https://doi.org/10.1021/acs.analchem.1c00805
Anal. Chem. 2021, 93, 7499−7507

Scheme 1. Working Principle of the RCA-CRISPR/Cas12a-Mediated Immobilization-Free Electrochemical Biosensing Platform for the Detection of miRNA-21: (A) In the Presence of miRNA-21 and (B) In the Absence of miRNA-21

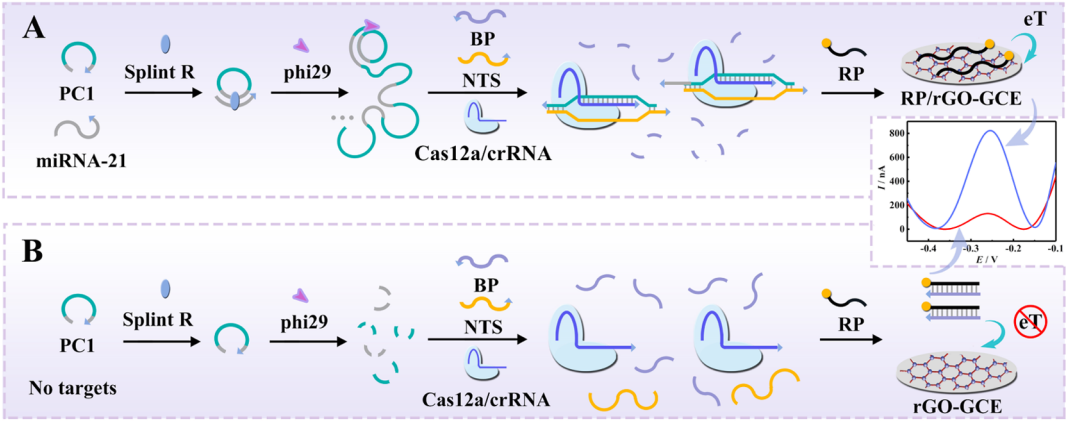

surface-bound probe is swayed, ascribing to the steric hindrance effect on the heterogeneous interface, resulting in decreased orientation/accessibility.[21−24] Particularly, these developed electrochemical biosensing platforms have a "signal-off" architecture, which is hard to provide guarantee for sensitivity and reproducibility because of limited signal gain and microenvironmental interferences from substrates and systems.[25] In view of the above, we are interested in developing an immobilization-free electrochemical biosensing platform that uses the CRISPR/Cas system as a biomolecular component for sensing-dependent response to overcome the above limitations. Given the programmability and integration of the CRISPR/Cas system, the combination of the CRISPR/Cas system with an immobilization-free electrochemical biosensing platform provides a new thinking for developing effective clinical diagnostic tools.

Herein, we extend the application of the CRISPR/Cas12a system to the immobilization-free electrochemical biosensing platform for the first time. By combining the rolling circle amplification (RCA) strategy, this electrochemical biosensor exhibits a "signal-on" model and achieves the highly sensitive and specific detection of microRNAs (miRNAs), the gene sequence of parvovirus B19 (PB-19), and adenosine-5′-triphosphate (ATP). Scheme 1 schematically shows the working principle of this immobilization-free electrochemical biosensing platform for the detection of miRNA-21 (Table S1). Recent studies demonstrated that the Cas12a enzyme harnesses indiscriminate single-stranded DNA (ssDNA) trans-cleavage activity, i.e., ssDNA substrates are cleaved into 2−4 nucleotide fragments, upon forming a complex with crRNA and its activator consisting of either trigger DNA strand (TS) alone or both of TS and nontrigger DNA strand (NTS).[7,26] In this strategy, the universal blocker probe (BP) is designed as the trans-cleavage substrate for the Cas12a enzymes. A universal reporter probe (RP) labeling with an electroactive substance (methylene blue in the 3′-terminal) is designed to hybridize with the BP. Typically, in the absence of targets, that is, the nonactivated Cas12a enzymes are unable to cut the BP, which will hybridize with the RP to form double-stranded DNA (dsDNA) that cannot be captured by the reduced graphene oxide-modified electrode (rGO/GCE), resulting in a negligible electrochemical signal. Conversely, upon recognizing the TS produced via RCA to assemble the Cas12a-crRNA-TS−NTS complex, the indiscriminate ssDNA trans-cleavage activity of Cas12a enzymes will be activated, resulting in the digestion of the BP. Thus, the free single-stranded RP labeling with methylene blue can be tightly adsorbed on the rGO/GCE through hydrophobic and $\pi-\pi$ stacking interactions,[27] leading to an obvious increased electrochemical signal. Significantly, the modular design of the components in RCA allows the use of the same CRISPR/Cas12a-crRNA, BP, and RP components, which lead to increased design compatibility. Therefore, the proposed immobilization-free electrochemical biosensing platform achieves the specific and sensitive detection of miRNA, PB-19, and ATP. Moreover, this RCA-CRISPR/Cas12a-based electrochemical biosensor exhibits a signal-on readout and is characterized by ease of use, cost-effectiveness, and flexibility, with the potential to develop point-of-care systems in clinical diagnosis.

EXPERIMENTAL SECTION

Preparation of Reduced Graphite Oxide (rGO)-Modified Electrode. Briefly, the exfoliated GO (10 mg) was soaked in 5 mL of ultrapure water and ultrasonicated for 2 h to obtain a GO suspension (2 mg mL^{-1}). Then, the GO suspension was centrifuged for 5 min at different rotational speeds (at 3000, 6000, 9000, 12000 rpm, respectively). The collected brown GO liquid supernatant was used in the whole experiment.

For the preparation of a reduced graphite oxide-modified glassy carbon electrode (rGO/GCE), the GCE was first polished with alumina powders (50 nm), then cleaned ultrasonically, and dried by blowing N_2. Next, the GO liquid supernatant (10 μL) was pipetted onto the clean GCE, followed by drying in a vacuum desiccator to prepare the GO/GCE. Finally, the GO/GCE was electrochemically reduced in 10 mM phosphate-buffered saline (PBS) (pH 5.0) using an $i-t$ amperometric curve procedure, in which the initial potential is −1.5 V, the sample interval is 0.1 s, and quiet time is 0 s. The prepared rGO/GCE was stored at room temperature for further experiment.

DNA Cleavage Assays. Generally, for the synthesis of the circular DNA template in a 20 μL system, 0.5 μM padlock probe 1 (PC 1) was annealed with various concentrations of miRNA-21 in 1× Splint R ligase reaction buffer at 55 °C for 10 min before the templated cyclization process. The ligation process was completed by incubating with 10 U Splint R ligase at 25 °C for 80 min, which was terminated by heat treatment (65 °C, 20 min) to obtain the circular DNA template (CDT). For the RCA reaction, 10 μL of the above prepared CDT was

https://doi.org/10.1021/acs.analchem.1c00805
Anal. Chem. 2021, 93, 7499−7507

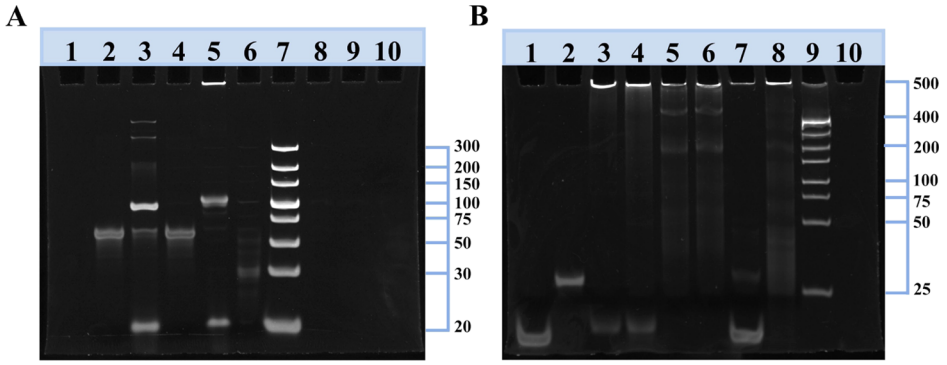

Figure 1. PAGE analysis of (A) miRNA-21-triggered RCA (lane 2: 1 μM PC 1, lane 3: 1 μM miRNA-21 + 0.5 μM PC 1 + 10 U Splint R ligase, lane 4: 0.5 μM PC 1 + 10 U Splint R ligase, lane 5: products in lane 3 + 10 U phi29 DNA polymerase, lane 6: products in lane 4 + 10 U phi29 DNA polymerase, lane 7: DNA marker (10−300 bp)) and (B) miRNA-21-activated RCA-CRISPR/Cas12a reaction (lane 1: BP, lane 2: NTS, lane 3: *t*RCA, lane 4: *t*RCA + Cas12a, lane 5: *t*RCA + Cas12a + crRNA, lane 6: *t*RCA + Cas12a + crRNA+BP, lane 7: *n*RCA + Cas12a + crRNA + NTS + BP, lane 8: *t*RCA + Cas12a + crRNA + NTS + BP, lane 9: DNA marker (25−500 bp)). The Cas12a, crRNA, NTS, and BP are at 100 nM, 120 nM, 1 μM, and 5 μM, respectively. The *t*RCA represents the products of RCA with miRNA-21, and the *n*RCA represents the products of RCA without miRNA-21.

incubated with phi29 DNA polymerase (5 μL, 2 U μL^{-1}), dNTPs (3 μL, 10 mM), and polymerase reaction buffer (2 μL, 10×). The reaction mixture was incubated at 30 °C for 1 h and then stopped by heat treatment (65 °C, 10 min). These products were then stored at −20 °C until use. For the DNA-templated cyclization of a padlock probe, the reaction was implemented with the Hi-T4 DNA ligase in 1× T4 ligase reaction buffer at 25 °C for 60 min. Finally, the reaction was terminated by heat treatment (65 °C, 10 min).

Generally, CRISPR/Cas12a cleavage assays were implemented in 1× NEBuffer 2.1. The preassembled Cas12a-crRNA (100/120 nM) was incubated with 10 μL of the activator (products of target-induced RCA), 1 μM NTS, and 5 μM single-stranded BP at 37 °C for 60 min, and then terminated by heat treatment (65 °C, 10 min). The products were stored at −20 °C until use.

Electrochemical Assay. Generally, 5 μL of RP (2 μM) was incubated with 5 μL of the products of CRISPR/Cas12a cleavage at 25 °C for 20 min, and then 10 μL of analyte solution was accurately sucked onto the surface of the rGO/GCE. Finally, the electrode was inserted into 10 mM Tris−HCl buffer (pH 7.0) for subsequent square wave voltammetry tests. The square wave voltammetry (SWV) tests were monitored at a pulse amplitude of 50 mV, an incremental potential of 4 mV with a frequency of 25 Hz over a potential range of −0.5 to 0 V. The cyclic voltammetry (CV) experiments were implemented in 10 mM PBS (100 mM NaCl, 5 mM $[Fe(CN)_6]^{3-/4-}$, pH 7.0) at different scan rates over the potential range of −0.2 to 0.6 V.

RESULTS AND DISCUSSION

Transformation of Targets. The biosensing platform involves three independent processes: transduction of the target recognition event into universal TS, the activation of the CRISPR/Cas system, and electrochemical detection. Cas12a (also named Cpf1) harnesses a single RuvC catalytic domain for crRNA-directed target DNA, followed by nonspecifically cleaving nearby ssDNA (named the collateral cleavage effect).[7,26] The critical process for the development of the CRISPR/Cas-mediated biosensor for miRNA, PB-19, and ATP detection is finding a solution to transform the target recognition event into the universal DNA fragments that perform as the TS of the Cas12a-crRNA complex. Therefore, we used the well-established RCA strategy to tackle the challenge.[28] As depicted in Scheme 1, the preamplification of target involves a padlock probe (PC) that is composed of two functional regions, in which region I (gray) is responsible for target recognition and region II (green) is a fragment complementary to the TS of the Cas12a-crRNA complex. In the absence of targets, the templated cyclization of PC cannot be implemented; therefore, the PC will be degraded gradually by phi29 DNA polymerase that possesses 3′−5′ single-stranded DNA exonucleolytic activity, resulting in no RCA amplicons. Conversely, in the presence of the targets, the targets actuate the cyclization of PC to form the circular DNA template (CDT), followed by directly primed RCA reaction along with the CDT to generate long DNA amplicons of a number of repeated segments with the TS sequence.

RCA-CRISPR/Cas12a-Based Immobilization-Free Electrochemical Biosensing Platform for MicroRNA Detection. MiRNAs are short noncoding RNAs with a length of ∼22 nucleotides, which play an important role in regulating the expression of other RNAs and have been demonstrated to be closely related to tumor growth or metastasis.[29,30] Therefore, the detection of cancer-associated miRNAs facilitates the prognosis, treatment, and monitoring of patients. Herein, miRNA-21 was taken as the model target to confirm the feasibility of the RCA-CRISPR/Cas12a-based immobilization-free electrochemical biosensing platform for miRNA detection. The feasibility of the transformation of the target recognition event into the universal TS through the RCA reaction was first evaluated by 12% nondenaturing polyacrylamide gel electrophoresis (PAGE) using Gel-Red as the fluorescence indicator (Figure 1A). The band in lane 2 represents the single-stranded PC. Compared with the mixture of PC and Splint R ligase (lane 4), the incubation of miRNA-21, PC, and Splint R ligase produces a characterized band of the CDT (lane 3), suggesting that miRNA-21 induced the templated cyclization of PC. Because of the enhanced steric hindrance, the CDT shows a higher molecular weight than PC. After the product in lane 4 is treated with the phi29 DNA polymerase, most of the characterized bands of the PC disappear due to the recognition and digestion of the PC from its 3′-terminus by phi29 DNA polymerase harboring 3′−5′ single-stranded DNA exonucleo-

https://doi.org/10.1021/acs.analchem.1c00805
Anal. Chem. 2021, 93, 7499−7507

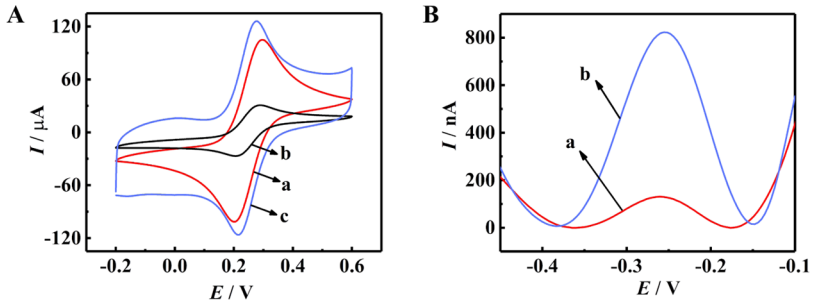

Figure 2. (A) CV characterization of (a) GCE, (b) GO/GCE, and (c) rGO/GCE; (B) SWV characterization of the feasibility of the biosensor for the detection of the miRNA-21: rGO/GCE response to the single-stranded RP treated with the products of the RCA-CRISPR/Cas12a reaction (a) in the absence of miRNA-21 and (b) in the presence of 10 pM miRNA-21.

lytic activity (lane 6). Conversely, the incubation of the products in lane 3 with phi29 DNA polymerase generates a bright and slower-moving band at the top of lane 5; meanwhile, the disappearance of the characterized bands of CDT is observed. Therefore, the results suggest that miRNA-21 activates the templated cyclization of PC to induce the successful RCA reaction.

The 12% nondenaturing PAGE using Gel-Red as the fluorescence indicator was further carried out to analyze the miRNA-21-activated RCA-CRISPR/Cas12a reaction (Figure 1B). The bands in lanes 1−3 represent the single-stranded BP, single-stranded NTS, and the products of miRNA-21-triggered RCA, respectively. Compared with the incubation of the products of miRNA-21-triggered RCA with the Cas12a enzyme (lane 4), treating this with the Cas12a-crRNA complex gives rise to the appearance of some new bands with low molecular weight (lane 5). This result reveals that binding of the Cas12a-crRNA to TS activates the Cas12a enzyme for site-specific DNA cutting to process the products of miRNA-21-triggered RCA into truncated TS. Using the single-stranded BP as the indicator, we tested the activated Cas12a enzyme for nonspecific ssDNA trans-cleavage. The characteristic band of the BP in lane 6 disappears, indicating that the binding of the Cas12a-crRNA to TS activates the Cas12a enzyme to perform nonspecific ssDNA trans-cleavage. When the Cas12a-crRNA complex binds to a dsDNA activator (TS/NTS), more new bands with low molecular weight are produced (lane 8), confirming that the Cas12a enzyme initiated by the dsDNA activator exhibits enhanced deoxyribonuclease activity,[7] whereas the characteristic band of the BP in lane 7 remains intact, suggesting that blocker cleavage occurs only when Cas12a-crRNA binds to the products of miRNA-21-triggered RCA. The above results demonstrate the feasibility of miRNA-21-activated RCA-CRISPR/Cas12a.

Electrochemical Characterization. Some electrochemical parameters, such as the effective surface area (A), current response (I), and potential difference (ΔE_p) were measured to evaluate the electrochemical characteristics of bare GCE, GO/GCE, and rGO/GCE. According to the equation,[31] the calculated A of the rGO/GCE (13.58×10^{-6} m^2, Figure S1C) showed a 1.5-fold improvement and 6.0-fold improvement compared with that of the bare GCE (9.18×10^{-6} m^2, Figure S1A) and GO/GCE (2.29×10^{-6} m^2, Figure S1B), respectively. This result indicates that more active sites are beneficial to the redox process of electroactive materials. This hypothesis was also verified by the cyclic voltammetry (CV) experiments in 5 mM ferricyanide and ferrocyanide solutions (Figure 2A). The anodic current response (I_{pa}) derived from the GO/GCE decreases to 33.7 μA (curve b) compared to the bare GCE (I_{pa} = 113.3 μA, curve a), indicating that the oxygen functionalities of GO on the electrode surface impede the interfacial electron transfer of $[Fe(CN)_6]^{3-/4-}$. When the oxygen functionalities (−COOH on the edge and C−O−C, −OH on the plane) of GO are reduced electrochemically, the I_{pa} increases to 111.8 μA (curve c), suggesting that rGO can accelerate interfacial charge transfer because of the restoration of the sp^2 carbon hybrid.[32] According to the calculated potential difference (ΔE_p) between anodic and cathodic peaks, the electron transfer efficiency of various material-modified electrodes was assessed (Figure 2A). The calculated ΔE_p values for the rGO/GCE, GO/GCE, and bare GCE are 61.0, 84.0, and 96.0 mV, respectively, indicating that the rGO/GCE possessed the highest electron transfer efficiency.

The signal transduction of the graphene-based electrochemical platform is dependent on the ability of graphene to distinguish between ssDNA and dsDNA. Therefore, the ability of graphene to distinguish between ssDNA and dsDNA was verified by CV tests (Figure S2). After the introduction of the single-stranded RP, a decreased redox peak current compared to that of the rGO/GCE is observed (curves a and b), implying that ssDNAs were captured by the rGO/GCE through $\pi-\pi$ interaction. However, introducing the single-stranded BP to hybridize with the single-stranded RP induces an increased redox peak current (curve c), indicating that dsDNA effectively hides its nucleobases in the helical structure for interacting with rGO. These characterization methods prove the successful preparation of the electrode.

Furthermore, the square wave voltammetry (SWV) tests were conducted to the feasibility of the RCA-CRISPR/Cas12a-based immobilization-free electrochemical biosensor for detecting miRNA-21 using methylene blue-labeled RP as the indicator (Figure 2B). An obviously increased SWV signal can be induced by miRNA-21 compared with that of the control group without miRNA-21. Collectively, by integrating RCA-CRISPR/Cas12a with graphene-based signal transduction, an immobilization-free electrochemical biosensing platform for the miRNA-21 assay is developed.

Spectroscopic Characterization. First, Fourier transform infrared (FT-IR) spectroscopy was adopted for the analysis of oxygen-containing groups of graphene (Figure S3). The spectrum of GO (curve a) exhibits characteristic absorption bands of C−O (ν(epoxy or alkoxy)), C═C, and C═O (ν(carbonyl)) at about 1053, 1635, and 1722 cm^{-1}, respectively. The bands of O−H (ν(carboxyl)) at about 1394 cm^{-1} and broad coupling ν(O−H) at about 3200 cm^{-1} are assigned to carboxylic acid, while the band at about 3411 cm^{-1}

https://doi.org/10.1021/acs.analchem.1c00805
Anal. Chem. 2021, 93, 7499−7507

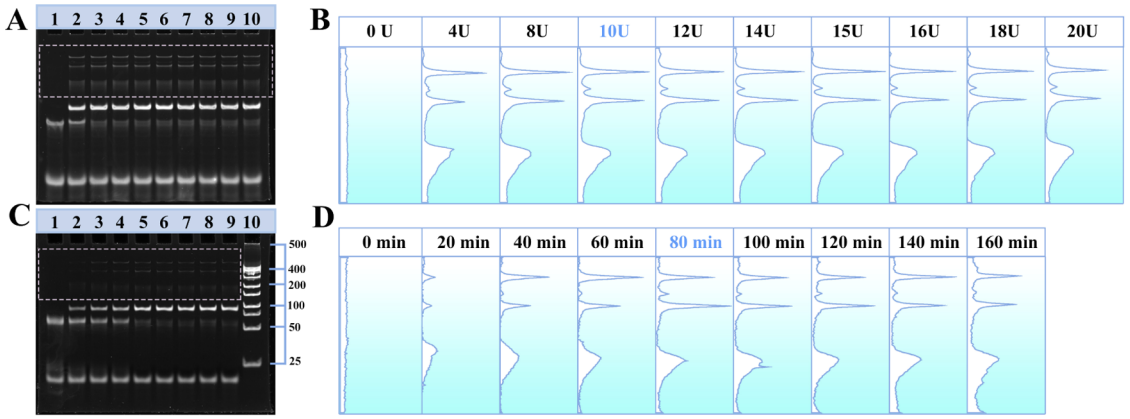

Figure 3. (A) Influence of the amounts of Splint R ligase on the formation of CDT: lanes 1−10 represent the reaction products of 1 μM miRNA-21 and 0.5 μM PC 1 with different amounts of Splint R ligase (from 0 to 20 U) respectively. (B) Grayscale intensity of the Gel-Red stained separated bands in (A). (C) Effect of the incubating time of cyclization of PC on the formation of CDT: lanes 1−9 represent the reaction products of 1 μM miRNA-21, 0.5 μM PC 1, and 10 U Splint R ligase in various time points (from 0 to 160 min). Lane 10 is DNA marker (25−500 bp). (D) Grayscale intensity of the Gel-Red stained separated bands in (C).

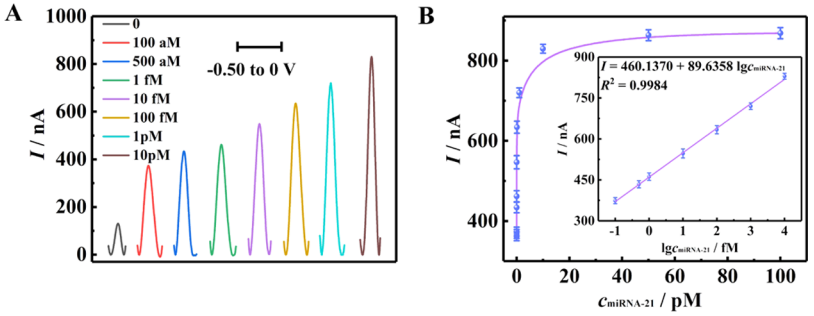

Figure 4. (A) SWV signal of the biosensor with various concentrations of miRNA-21 (from 0 M to 10 pM); (B) change of the I with the concentration of miRNA-21 in the range of 10 aM to 100 pM. The inset shows the linear relationship of I vs the logarithm of the miRNA-21 concentration in the range of 100 aM to 10 pM.

can be attributed to the O−H stretching mode of intercalated water. After GO was treated with electrochemical reduction, the oxygen-containing groups (C═O, C−O (ν(epoxy or alkoxy)), and O−H (ν(carboxyl))) were greatly weakened.[32,33]

Then, the electronic and structural properties of GO and rGO were investigated via Raman spectroscopy (Figure S4). The Raman spectrum of GO exhibits a typical G band at 1587 cm^{-1} and a D band at 1347 cm^{-1}, while that of rGO shows a G band at about 1587 cm^{-1} and a D band at 1343 cm^{-1}. The intensity ratio of the D band to the G band (I_D/I_G) of rGO relative to that of GO is increased, revealing that the average size of the sp^2 network decreases during the reduction process.[34] Interestingly, the I_D/I_G values of rGO increase with the reduction time from 0 to 50 s (Figure S5). As the reduction time increases, the I_D/I_G values of rGO decrease and then level off. Therefore, the optimal reduction time is 50 s.

Optimization of Experimental Conditions. The critical step of the miRNA-21-triggered RCA-CRISPR/Cas12a reaction is the templated cyclization of PC that is implemented with Splint R ligase. The amount of Splint R ligase and the reaction time are important factors affecting the yield of CDT. Therefore, we first performed 12% PAGE to optimize the amount of Splint R ligase. As shown in Figure 3A, lanes 1−10 represent the reaction products of miRNA-21-templated cyclization of PC in the presence of various amounts of Splint R ligase. Compared with the band in lane 1, some new bands corresponding to the characterized band of the CDT are observed (from lanes 2 to 10), suggesting that miRNA-21 induced the templated cyclization of PC. For ease of quantification, the intensity of the Gel-Red stained bands in the dotted box was transformed into the curve chart via ImageJ software. The peak area increases with the increased amount of Splint R ligase and levels off at 10 U (Figure 3B). Therefore, the amount of 10 U was chosen for the subsequent experiment. Then, the reaction time of the templated cyclization of PC was also optimized. Lanes 1−9 represent the reaction products of miRNA-21-templated cyclization of PC at different time points (Figure 3C). In contrast to the band in lane 1, some higher molecular bands generate in lanes 2−9, demonstrating the formation of CDT. In addition, the intensity of the bands corresponding to the characterized band of CDT was estimated using ImageJ software. The peak area increases with the extension of reaction time and levels off at 80 min (Figure 3D). Thus, the optimal incubating time of templated cyclization of PC is 80 min.

The electron conductivity of the graphene-based electrochemical platform is related to the graphene film; thus, the concentration of the GO suspension used for preparing the graphene film was also optimized. Four different concentrations of the GO suspension (1, 2, 3, and 5 mg mL^{-1}) have been prepared for making four graphene-modified electrochemical sensors using the same procedure. The CV response was used as an indicator to assess the conductivity of the rGO film. As displayed in Figure S6, the I_{pa} of the rGO film made of

https://doi.org/10.1021/acs.analchem.1c00805
Anal. Chem. 2021, 93, 7499−7507

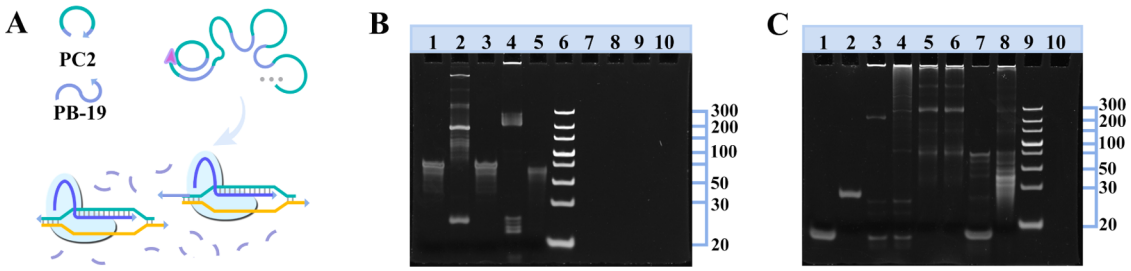

Figure 5. (A) Schematic illustration of the PB-19-activated RCA-CRISPR/Cas12a; PAGE analysis of (B) PB-19-triggered RCA (lane 1: 1 μM PC 2, lane 2: 1 μM PB-19 + 0.5 μM PC 2 + 9 U Hi-T4 ligase, lane 3: 0.5 μM PC 2 + 9 U Hi-T4 ligase, lane 4: products in lane 2 + 10 U phi29 DNA polymerase, lane 5: products in lane 3 + 10 U phi29 DNA polymerase, lane 6: DNA marker (10−300 bp)); and (C) PB-19-activated RCA-CRISPR/Cas12a reaction (lane 1: BP, lane 2: NTS, lane 3: *t*RCA, lane 4: *t*RCA + Cas12a, lane 5: *t*RCA + Cas12a + crRNA, lane 6: *t*RCA + Cas12a + crRNA + BP, lane 7: *n*RCA + Cas12a + crRNA + NTS + BP, lane 8: *t*RCA + Cas12a + crRNA + NTS + BP, lane 9: DNA marker (10−300 bp)). The Cas12a, crRNA, NTS, and BP are at 100 nM, 120 nM, 1 μM, and 5 μM, respectively. The *t*RCA represents the products of RCA with PB-19, and the *n*RCA represents the products of RCA without PB-19.

2 mg mL^{-1} GO suspension is the strongest compared to the rGO film made of other concentrations of the GO suspension (1, 3, and 5 mg mL^{-1}). Therefore, 2 mg mL^{-1} GO suspension was used in further experiments.

Analytical Performance. To further evaluate the performance of the RCA-CRISPR/Cas12a-based immobilization-free electrochemical biosensor, the dynamic response of the biosensor to various concentrations of synthetic miRNA-21 was measured via SWV. Figure 4A depicts that the SWV signal of methylene blue gradually increased with the increasing miRNA-21 concentration from 0 M to 10 pM. Figure 4B shows the linear relationship of the current intensity (I) with the increasing concentrations of miRNA-21 on the logarithmic scale, and the limit of detection (LOD) calculated according to the IUPAC definition (see the Supporting Information for details) is 0.83 aM, which is superior in analytical performance to other recently reported strategies (Table S2).

Specificity, Reproducibility, Stability, and Practicability of the Biosensor. The selectivity of the RCA-CRISPR/Cas12a-based immobilization-free electrochemical biosensor was evaluated by distinguishing miRNA-21 from other potential interfering miRNAs, including miRNA-122, miRNA-141, miRNA-200c, and miRNA-155 (Figure S7). A negligible difference of the SWV current response between the interfering miRNAs and blank samples was observed, while the SWV current in response to miRNA-21 shows an obvious increase. These results indicate that this biosensor exhibits high selectivity. Next, inter-assays and intra-assays were performed to assess the reproducibility of the RCA-CRISPR/Cas12a-based immobilization-free electrochemical biosensor. The relative standard deviations (RSDs) of this biosensor are 8.53% (n = 5) for inter-assays and 3.21% (n = 5) for intra-assays, respectively, suggesting that the developed biosensor exhibits a satisfactory reproducibility. To evaluate the stability of this biosensor, storage experiments were performed via measuring the storage solution at intervals of 2 days using the same rGO-modified electrodes. The change in the current exhibits little fluctuation after 5-times SWV tests, and the SWV current decreases by 5.92%, demonstrating that the biosensor had good stability.

In addition, to assess the potential of the RCA-CRISPR/Cas12a-based immobilization-free electrochemical biosensor in real samples, the recovery experiments were implemented via spiking known concentrations of miRNA-21 (500 aM, 10 fM, and 1 pM, respectively) in 10-fold diluted healthy people serum. As shown in Table S3, the recoveries of this biosensor for miRNA-21 detection were 97.24, 99.39, and 106.21%, respectively, suggesting that the RCA-CRISPR/Cas12a-based immobilization-free electrochemical biosensor is desirable for sensitive analysis in relatively complex biological samples.

RCA-CRISPR/Cas12a-Based Immobilization-Free Electrochemical Biosensing Platform for DNA Detection. Parvovirus B19, a small and single-stranded DNA virus without an envelope, causes erythema infectiosum in pregnant women and children.[35,36] It is a common virus that causes community-acquired respiratory diseases. We further studied the analytical performance of the RCA-CRISPR/Cas12a-based immobilization-free electrochemical biosensor for Parvovirus B19 DNA (PB-19). As illustrated in Figure 5A, the straightforward PB-19 detection was achieved via transformation of the gene sequence into the universal TS of the Cas12a-crRNA complex by RCA. The feasibility of PB-19-triggered RCA was first verified by 12% nondenaturing PAGE using Gel-Red as the fluorescence indicator (Figure 5B). The results of electrophoretic analysis demonstrated that long DNA amplicons containing a number of repeated TS segments were produced. In addition, the PB-19-activated CRISPR/Cas12a was further analyzed by 12% nondenaturing PAGE using the single-stranded BP as a reporter (Figure 5C). Based on the ability of graphene to distinguish between ssDNA and dsDNA, the RCA-CRISPR/Cas12a-based immobilization-free electrochemical biosensor can detect PB-19 in a signal-on detection format. Figure S8A shows that the SWV signal of methylene blue increased with the increasing concentration of PB-19 from 0 M to 10 pM. A linear range of 50 aM to 10 pM and an LOD of 0.52 aM were obtained according to the IUPAC definition (see the Supporting Information for details) (Figure S8B).

To further investigate the selectivity of the RCA-CRISPR/Cas12a-based immobilization-free electrochemical biosensor, base mismatched sequences were applied to challenge this electrochemical biosensor. The SWV response induced by scrambled sequences was negligible compared with that induced by PB-19 (Figure S9), suggesting a good selectivity of the biosensor in differentiating PB-19 from nontargets.

RCA-CRISPR/Cas12a-Based Immobilization-Free Electrochemical Biosensing Platform for Non-Nucleic Acid Target Detection. Since both RCA and CRISPR/Cas12a processes are based on nucleic acids as conversion elements, the key to the design is to find a common strategy for transforming non-nucleic acid targets into nucleic acids. Combining the aptamers and the antisense displacement strategy that utilizes competitive binding between the double-

https://doi.org/10.1021/acs.analchem.1c00805
Anal. Chem. 2021, 93, 7499−7507

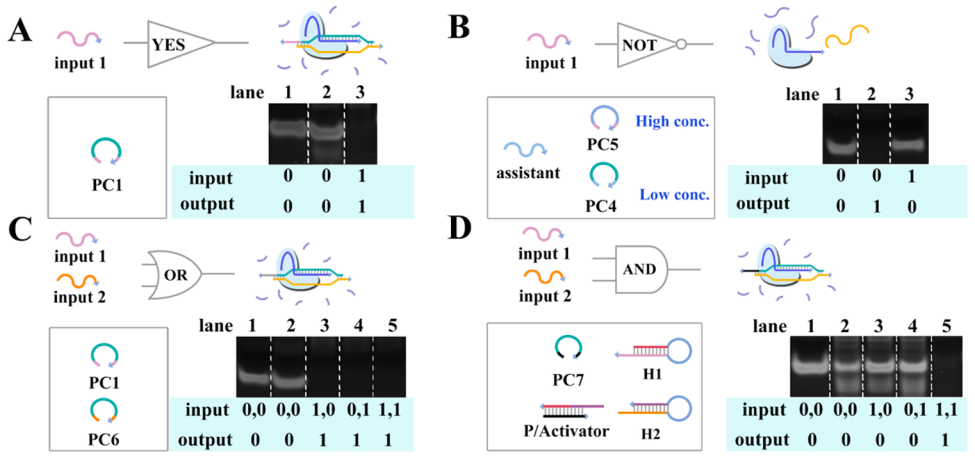

Figure 6. Logic computation with the RCA-CRISPR/Cas12a system: reaction set-up and 12% PAGE results for (A) YES gate, (B) NOT gate, (C) OR gate, (D) AND gate. In all experiments, input and PC were fixed at 1 and 0.5 μM, respectively. The final concentrations of hairpins and P/Activator for AND gate were 0.25 μM.

stranded primer/aptamer and small molecules, we constructed the RCA-CRISPR/Cas12a-based immobilization-free electrochemical biosensing platform for small molecule detection of interest. Adenosine-5′-triphosphate (ATP) serves as the signal molecule and energy carrier in cellular processes, whose level can be used as an indicator for some diseases.[37,38] Therefore, we chose ATP as the target to explore whether the RCA-CRISPR/Cas12a-based immobilization-free electrochemical biosensor can detect small molecules. As illustrated in Figure S10A, in the absence of the ATP, the primer hybridizes with the aptamer to prevent it from binding to the PC, resulting in the nonactivated CRISPR/Cas12a system. Upon introducing ATP, ATP binds to its aptamer to release the primer; therefore, the primer can hybridize PC to induce its templated cyclization. As a result, the ATP-triggered RCA activates the Cas12a enzyme for nonspecific ssDNA trans-cleavage.

The feasibility of the ATP-activated RCA-CRISPR/Cas12a reaction was first verified by 12% nondenaturing PAGE using Gel-Red as the fluorescence indicator (Figure S10B). The electrophoretic results demonstrated that ATP can activate the Cas12a enzyme for the single-stranded BP cleavage compared to the conditions without ATP. We then measured the SWV response to different concentrations of ATP diluted with DEPC-treated water to assess the aptamer-regulated RCA-CRISPR/Cas12a biosensor for detecting ATP quantitatively (Figure S11A). The developed RCA-CRISPR/Cas12a-based immobilization-free electrochemical biosensor exhibits a good linear relationship with ATP concentration in the range from 10 pM to 100 nM (Figure S11B). According to the IUPAC definition (see the Supporting Information for details), the calculated LOD is 0.46 pM, and the square of the correlation coefficient is 0.9966. A comparison of the sensitivity for the detection of ATP between the RCA-CRISPR/Cas12a-based immobilization-free electrochemical biosensor and other platforms is listed in Table S4. Due to the extremely high affinity and specificity of aptamer toward ATP, the RCA-CRISPR/Cas12a-based immobilization-free electrochemical biosensor can discriminate guanosine-5′-monophosphate (GMP), adenosine-5′-triphosphate (ATP), adenosine-5′-diphosphate (ADP), and adenosine-5′-monophosphate (AMP) (Figure S12). Moreover, the anti-interference capability of this biosensor was assessed by utilizing the mixture of ATP and interfering substances (ADP, AMP, GMP) as the target. The measured SWV current response is comparable with that of ATP alone. These results indicate that this biosensor exhibits high selectivity and anti-interference capability. To explore the potential use of the RCA-CRISPR/Cas12a-based immobilization-free electrochemical biosensor in complex samples, 10-fold diluted serum spiked with various concentrations of ATP was tested (Table S5). The recovery rate ranges from 95 to 104%, suggesting that the RCA-CRISPR/Cas12a-based immobilization-free electrochemical biosensor has potential application in clinical isolates.

Logic Computation Circuits. This programmability of the RCA reaction to convert arbitrary inputs into the universal TS for the Cas12a-crRNA complex presents a modular framework for engineering DNA circuits for complex tasks. Accurate signal processing of inputs through DNA logic circuits has been demonstrated as a valuable architecture regarding programming complex dynamic molecular behavior.[39,40] We subsequently show how the RCA-CRISPR/Cas12a system can be used to construct YES, NOT, AND, and OR logic for arbitrary inputs. The basic strategy is to transduce the input sequence into TS of the Cas12a-crRNA complex via the RCA reaction, activate the collateral cleavage effect of the Cas12a enzyme, and read out the results via 12% PAGE using the single-stranded BP as the indicator.

Figure 6A shows the design of a YES gate for input 1, which is implemented with the typical RCA reaction introduced in the previous section (Scheme 1). After incubation of the input 1-induced preamplification products with the Cas12a-crRNA complex, the characteristic band of the single-stranded BP disappeared (lane 3). However, if no input 1 is present, the collateral cleavage effect of the Cas12a enzyme cannot be activated and a bright band corresponding to the single-stranded BP was observed (lanes 1 and 2).

The separation of timescales between the input 1-dependent and assistant-dependent RCA reaction was performed to implement NOT logic (Figure 6B). In this system, the PC 4 contains two functional regions, where region I (gray) is complementary to the assistant, and region II (green) is the complementary sequence of TS. Another PC 5 also consists of two functional regions, in which region I (pink) is responsible for input 1 recognition, but region II (blue) is an arbitrary fragment that is not complementary to TS. Note that the input 1-dependent PC 5 at a much higher concentration than the

https://doi.org/10.1021/acs.analchem.1c00805
Anal. Chem. 2021, 93, 7499−7507

assistant-dependent PC 4 evaluates to True. Thus, if input 1 is inputted, the PC 5-templated RCA products are unable to trigger the collateral cleavage effect of the Cas12a enzyme. However, if no input 1 is inputted, all of the assistants will trigger the templated cyclization of PC 4 at a slow rate; therefore, the assistant-triggered RCA products will activate the collateral cleavage effect of the Cas12a enzyme. This gate is validated by comparing the characteristic band of the single-stranded BP in the case of without (lane 2) and with (lane 3) input 1, respectively.

The OR gate for two inputs works as shown in Figure 6C. The OR gate consists of two padlock probes (PC 1 and PC 6), where region II (green) is the complementary sequence of TS, region I (pink) in PC 1 is the recognition sequence of input 1, and region I (orange) in PC 6 is complementary to input 2. Each input can trigger the templated cyclization of the corresponding PC, and when one or both of the two PCs are triggered, the RCA reaction can generate a large amount of TS to activate the collateral cleavage effect of the Cas12a enzyme. This gate is validated with 12% PAGE (Figure 6D), which shows a bright band corresponding to the characteristic band of the single-stranded BP when neither input is inputted (lane 2). Rather, if one or both two inputs are inputted, the characteristic band of the single-stranded BP disappeared (lanes 3−5).

The design of AND logic gate responding to two inputs is inspired by the target-responsive DNA three-way junction (TWJ) strategy.[41] This computation is achieved by the introduction of two hairpin probes (HP), which consist of the target recognition region (i), bridging region (ii), and semiprimer region (iii). The target recognition region (i) in HP1 is responsible for input 1 and that in HP2 is used to hybridize with input 2 (Figure S13). The bridging domain with 12 bases between H1 and HP2 are designed in the loop of H, but a stable duplex structure cannot form if neither input is inputted (lane 2) or if just one input is inputted (lanes 3 and 4). Only when two inputs are inputted, the H will be unfolded, and the bridging domain between HP1 and HP2 will hybridize to each other to form a stable TWJ structure. Therefore, the formed TWJ brings semiprimer between HP1 and HP2 into close proximity, which can trigger a subsequent RCA reaction. The characteristic band of the single-stranded BP disappeared in the gel, suggesting successful evaluation of the AND logic (lane 5).

These DNA logic circuits demonstrate the modularity and programmability of the stimuli-responsive RCA-CRISPR/Cas12a, which in principle can adapt to any single-stranded DNA or RNA inputs, even though any single-stranded DNA is transformed by a non-nucleic acid target. In addition, we predict that the stimuli-responsive RCA-CRISPR/Cas12a can be compatible with various readout techniques to construct DNA circuits for complex tasks.

CONCLUSIONS

In summary, this work presents an immobilization-free electrochemical biosensing platform with high sensitivity and selectivity, especially programmability and universal applicability, coupling modular RCA with the CRISPR/Cas12a system. Given the programmability and integration of the RCA and CRISPR/Cas12a system, the generality of RCA-CRISPR/Cas12a toward miRNAs, DNA, and small molecules is easily implemented by simply adjusting the regions for target recognition in RCA components. The modularity and programmability of the stimuli-responsive RCA-CRISPR/Cas12a system have been experimentally demonstrated via constructing DNA logic circuits (YES, NOT, OR, AND) of DNA inputs, which suggests that the RCA-CRISPR/Cas12a system has the potential in implementing complex tasks. Although RCA-CRISPR/Cas12a amplification is carried out in two steps, the detection step is free of probe surface immobilization, which is beneficial for simplifying the operation and saving time. In addition, the RCA-CRISPR/Cas12a-based electrochemical biosensor exhibits signal-on readout and has other advantages such as ease of use, low cost, and flexibility. Therefore, this work broadens the application of the CRISPR/Cas12a system to the immobilization-free electrochemical biosensing platform and provides a valuable tool for bioanalytical and biomedical applications.

ASSOCIATED CONTENT

Supporting Information

The Supporting Information is available free of charge at https://pubs.acs.org/doi/10.1021/acs.analchem.1c00805.

Chemicals and reagents; apparatus and measurements; native polyacrylamide gel electrophoresis; calculation of the effective surface area of the modified electrode; calculation of limit of detection; and additional figures and tables (PDF)

AUTHOR INFORMATION

Corresponding Authors

Hong Qun Luo − *Key Laboratory of Luminescence Analysis and Molecular Sensing, School of Chemistry and Chemical Engineering, Southwest University, Chongqing 400715, P. R. China*; orcid.org/0000-0002-2254-6034; Email: luohq@swu.edu.cn

Nian Bing Li − *Key Laboratory of Luminescence Analysis and Molecular Sensing, School of Chemistry and Chemical Engineering, Southwest University, Chongqing 400715, P. R. China*; orcid.org/0000-0001-6395-2074; Email: linb@swu.edu.cn

Authors

Min Qing − *Key Laboratory of Luminescence Analysis and Molecular Sensing, School of Chemistry and Chemical Engineering, Southwest University, Chongqing 400715, P. R. China*

Sheng Liang Chen − *Key Laboratory of Luminescence Analysis and Molecular Sensing, School of Chemistry and Chemical Engineering, Southwest University, Chongqing 400715, P. R. China*

Zhe Sun − *Key Laboratory of Luminescence Analysis and Molecular Sensing, School of Chemistry and Chemical Engineering, Southwest University, Chongqing 400715, P. R. China*

Yi Fan − *Key Laboratory of Luminescence Analysis and Molecular Sensing, School of Chemistry and Chemical Engineering, Southwest University, Chongqing 400715, P. R. China*

Complete contact information is available at: https://pubs.acs.org/10.1021/acs.analchem.1c00805

Author Contributions

All authors have approved the final version of the manuscript.

https://doi.org/10.1021/acs.analchem.1c00805
Anal. Chem. 2021, 93, 7499−7507

Notes

The authors declare no competing financial interest.

■ ACKNOWLEDGMENTS

The authors gratefully acknowledge support from the National Natural Science Foundation of China (No. 21675131) and the Natural Science Foundation of Chongqing (No. cstc2020jcyj-zdxmX0003).

■ REFERENCES

(1) Kelley, S. O. *Acc. Chem. Res.* **2017**, *50*, 503−507.
(2) Dai, Y. F.; Liu, C. C. *Angew. Chem., Int. Ed.* **2019**, *58*, 12355−12368.
(3) Li, Y.; Li, S. Y.; Wang, J.; Liu, G. Z. *Trends Biotechnol.* **2019**, *37*, 730−743.
(4) Dai, Y. F.; Wu, Y. F.; Liu, G. Z.; Gooding, J. J. *Angew. Chem., Int. Ed.* **2020**, *59*, 20754−20766.
(5) Gootenberg, J. S.; Abudayyeh, O. O.; Lee, J. W.; Essletzbichler, P.; Dy, A. J.; Joung, J.; Verdine, V.; Donghia, N.; Daringer, N. M.; Freije, C. A.; Myhrvold, C.; Bhattacharyya, R. P.; Livny, J.; Regev, A.; Koonin, E. V.; Hung, D. T.; Sabeti, P. C.; Collins, J. J.; Zhang, F. *Science* **2017**, *356*, 438.
(6) Li, S. Y.; Cheng, Q. X.; Liu, J. K.; Nie, X. Q.; Zhao, G. P.; Wang, J. *Cell Res.* **2018**, *28*, 491−493.
(7) Chen, J. S.; Ma, E. B.; Harrington, L. B.; Da Costa, M.; Tian, X. R.; Palefsky, J. M.; Doudna, J. A. *Science* **2018**, *360*, 436.
(8) Huang, M. Q.; Zhou, X. M.; Wang, H. Y.; Xing, D. *Anal. Chem.* **2018**, *90*, 2193−2200.
(9) Peng, S.; Tan, Z.; Chen, S. Y.; Lei, C. Y.; Nie, Z. *Chem. Sci.* **2020**, *11*, 7362−7368.
(10) Wang, Y. Q.; Ke, Y. Q.; Liu, W. J.; Sun, Y. Q.; Ding, X. T. *ACS Sens.* **2020**, *5*, 1427−1435.
(11) Zhou, W. H.; Hu, L.; Ying, L. M.; Zhao, Z.; Chu, P. K.; Yu, X. F. *Nat. Commun.* **2018**, *9*, No. 5012.
(12) Chen, X. L.; Wu, Y. W.; Cao, G. H.; Wang, X. F.; Ji, Z.; Huo, D. Q.; Xu, F. L.; Hou, C. J. *ACS Sens.* **2020**, *5*, 1615−1623.
(13) Chen, Q.; Tian, T.; Xiong, E. H.; Wang, P.; Zhou, X. M. *Anal. Chem.* **2020**, *92*, 573−577.
(14) Li, H.; Li, M. L.; Yang, Y. C.; Wang, F.; Wang, F.; Li, C. *Anal. Chem.* **2021**, *93*, 3209−3216.
(15) Dai, Y.; Somoza, R. A.; Wang, L.; Welter, J. F.; Li, Y.; Caplan, A. I.; Liu, C. C. *Angew. Chem., Int. Ed.* **2019**, *58*, 17399−17405.
(16) Zhang, D. C.; Yan, Y. R.; Que, H. Y.; Yang, T. T.; Cheng, X. X.; Ding, S. J.; Zhang, X. M.; Cheng, W. *ACS Sens.* **2020**, *5*, 557−562.
(17) Xu, W.; Jin, T.; Dai, Y. F.; Liu, C. C. *Biosens. Bioelectron.* **2020**, *155*, No. 112100.
(18) Xuan, F.; Fan, T. W.; Hsing, I. M. *ACS Nano* **2015**, *9*, 5027−5033.
(19) Wu, J.; Campuzano, S.; Halford, C.; Haake, D. A.; Wang, J. *Anal. Chem.* **2010**, *82*, 8830−8837.
(20) Ge, L.; Wang, W. X.; Li, F. *Anal. Chem.* **2017**, *89*, 11560−11567.
(21) Zhao, L. H.; Qi, X. Y.; Yan, X. C.; Huang, Y. F.; Liang, X. G.; Zhang, L. Q.; Wang, S.; Tan, W. H. *J. Am. Chem. Soc.* **2019**, *141*, 17493−17497.
(22) Monserud, J. H.; Schwartz, D. K. *ACS Nano* **2014**, *8*, 4488−4499.
(23) Watkins, H. M.; Vallée-Bélisle, A.; Ricci, F.; Makarov, D. E.; Plaxco, K. W. *J. Am. Chem. Soc.* **2012**, *134*, 2120−2126.
(24) Mason, S. D.; Wang, G. A.; Yang, P.; Li, Y. Y.; Li, F. *ACS Nano* **2019**, *13*, 8106−8113.
(25) Li, L. D.; Mu, X. J.; Peng, Y.; Chen, Z. B.; Guo, L.; Jiang, L. *Anal. Chem.* **2012**, *84*, 10554−10559.
(26) Swarts, D. C.; van der Oost, J.; Jinek, M. *Mol. Cell* **2017**, *66*, 221−233.
(27) Ganguli, A.; Faramarzi, V.; Mostafa, A.; Hwang, M. T.; You, S. Y.; Bashir, R. *Adv. Funct. Mater.* **2020**, *30*, No. 2001031.
(28) Mohsen, M. G.; Kool, E. T. *Acc. Chem. Res.* **2016**, *49*, 2540−2550.
(29) Slack, F. J.; Chinnaiyan, A. M. *Cell* **2019**, *179*, 1033−1055.
(30) Hayes, J.; Peruzzi, P. P.; Lawler, S. *Trends Mol. Med.* **2014**, *20*, 460−469.
(31) Bard, A. J.; Faulkner, L. R. *Electrochemical Methods: Fundamentals and Applications*, 2nd ed.; Wiley: New York, 2001.
(32) Guo, H. L.; Wang, X. F.; Qian, Q. Y.; Wang, F. B.; Xia, X. H. *ACS Nano* **2009**, *3*, 2653−2659.
(33) Zhu, C. Z.; Guo, S. J.; Fang, Y. X.; Dong, S. J. *ACS Nano* **2010**, *4*, 2429−2437.
(34) Fan, Z. J.; Kai, W.; Yan, J.; Wei, T.; Zhi, L. J.; Feng, J.; Ren, Ym.; Song, L. P.; Wei, F. *ACS Nano* **2011**, *5*, 191−198.
(35) Sanchez, J. L.; Romero, Z.; Quinones, A.; Torgeson, K. R.; Horton, N. C. *Biochemistry* **2016**, *55*, 6577−6593.
(36) Leisi, R.; von Nordheim, M.; Kempf, C.; Ros, C. *Bioconjugate Chem.* **2015**, *26*, 1923−1930.
(37) Tanaka, K.; Gilroy, S.; Jones, A. M.; Stacey, G. *Trends Cell Biol.* **2010**, *20*, 601−608.
(38) Ferrer, I.; Perez, E.; Dalfó, E.; Barrachina, M. *Neurosci. Lett.* **2007**, *415*, 205−209.
(39) Song, T.; Eshra, A.; Shah, S.; Bui, H.; Fu, D.; Yang, M.; Mokhtar, R.; Reif, J. *Nat. Nanotechnol.* **2019**, *14*, 1075−1081.
(40) Wang, W. J.; Huang, S.; Li, J. J.; Rui, K.; Bi, S.; Zhang, J. R.; Zhu, J. J. *Chem. Sci.* **2017**, *8*, 174−180.
(41) Li, F.; Lin, Y. W.; Le, X. C. *Anal. Chem.* **2013**, *85*, 10835−10841.

https://doi.org/10.1021/acs.analchem.1c00805
Anal. Chem. 2021, 93, 7499−7507